

## Towards canonical adverse-pressure-gradient turbulent boundary layers

**Ramis Örlü**

Linné FLOW Centre  
KTH Mechanics  
Stockholm, Sweden  
ramis@mech.kth.se

**Ricardo Vinuesa**

Linné FLOW Centre  
KTH Mechanics  
Stockholm, Sweden  
rvinuesa@mech.kth.se

**Carlos Sanmiguel Vila**

Aerospace Engineering Group  
University Carlos III of Madrid  
Leganés, Spain  
csanmigu@ing.uc3m.es

**Stefano Discetti**

Aerospace Engineering Group  
University Carlos III of Madrid  
Leganés, Spain  
sdiscett@ing.uc3m.es

**Andrea Ianiro**

Aerospace Engineering Group  
University Carlos III of Madrid  
Leganés, Spain  
aianiro@ing.uc3m.es

**Philipp Schlatter**

Linné FLOW Centre  
KTH Mechanics  
Stockholm, Sweden  
pschlatt@mech.kth.se

### ABSTRACT

The present investigation focuses on the concerted investigation of pressure gradient and streamwise curvature effects on turbulent boundary layers. In particular, a number of direct and large-eddy simulations covering a wide range of pressure gradient parameters and streamwise histories on flat and curved surfaces is performed and will be compared with wind-tunnel experiments utilising hot-wire anemometry and particle image velocimetry that overlap and extend the Reynolds number range. Results are aimed at isolating the effects of pressure gradients, streamwise curvature and streamwise (pressure gradient) histories as well as Reynolds number, which have traditionally inhibited to draw firm conclusions from the available data.

### MOTIVATION

The quest for more efficient airplanes, trains and other ground vehicles is directly coupled to reducing the form and/or friction drag without compromising the other. A prototype of a canonical flow on which our understanding of friction drag has been developed is the zero-pressure gradient (ZPG) turbulent boundary layer (TBL). Despite its importance for fundamental research, most flows of relevance in technical applications are exposed to various pressure gradients and surface curvature which instead may lead to changes of the form drag. The applicability of knowledge from canonical wall-bounded flows is hence limited when it comes to these complex flows and geometries (see e.g. Patel & Sotiropoulos, 1997). Although a number of simulations (see e.g. Lee & Sung, 2008) and experiments (see e.g. Monty *et al.*, 2011) on e.g. adverse pressure gradient (APG) TBLs, spanning a wide range of Reynolds numbers  $Re$  and values of the Clauser pressure-gradient parameter  $\beta = \delta^*/\tau_w dP_e/dx$  (where  $\delta^*$  is the displacement thickness,  $\tau_w$  the mean wall-shear stress and  $dP_e/dx$  is the streamwise pressure gradient) have been performed in the past, it is hard to draw firm conclusions from the available data. One of the reasons explaining the difficulties in comparing the various datasets is the differently varying streamwise distributions of  $\beta$ , i.e. the different upstream histories leading to a particular pressure-gradient condition. The importance of inflow and tripping effects has also been reemphasised in the case of ZPG TBLs (Schlatter & Örlü, 2012; Sanmiguel Vila *et al.*, 2017b), and it is therefore anticipated, that development effects are more complex and more crucial for APG TBLs. The present contribution aims therefore at establishing different upstream histories on APG TBLs both through simulations and experiments, and in

particular to maintain a region of constant  $\beta$ , in order to study the genuine effect of the imposed pressure gradient and its upstream history separately.

Since the effect of the pressure gradient on the TBL is closely related to its streamwise development, it is important to define the concept of an *equilibrium* boundary layer: according to the strict definition by Townsend (1956), this condition requires the mean flow and Reynolds-stress tensor profiles to be independent of the streamwise position  $x$ , when scaled with appropriate local velocity and length scales. As also shown by Townsend (1956) this condition is only satisfied by the sink flow, although it is possible to define a less restrictive *near-equilibrium* condition when the mean velocity defect  $U_\infty - U$  is self-similar in the outer region, which in any case dominates at high Reynolds numbers (Marusic *et al.*, 2010). Townsend (1956) and Mellor & Gibson (1966) showed that these near-equilibrium conditions can be obtained when the freestream velocity is prescribed by a power law such that  $U_\infty = C(x - x_0)^m$ , where  $C$  is a constant,  $x_0$  is a virtual origin and  $m$  the power-law exponent. In particular, Townsend (1956) showed that  $m$  has to be larger than  $-1/3$  in order to obtain near-equilibrium conditions, which means that all accelerated TBLs subjected to a favorable pressure gradient (FPG), with  $U_\infty$  distributions defined by a power law, exhibit near-equilibrium. Regarding TBLs subjected to APGs, only the ones with  $U_\infty$  defined by a power law as defined above, and satisfying  $-1/3 < m < 0$  are in near-equilibrium conditions. Further discussion on equilibrium in APG TBLs can be found in the work by Maciel *et al.* (2006).

### NUMERICAL AND EXPERIMENTAL DATABASES

For the present study, use is being made of a number of direct numerical and large-eddy simulations (DNS and LES) in flat-plate ZPG (Schlatter & Örlü, 2010; Schlatter & Örlü, 2012) and APG (Bobke *et al.*, 2016, 2017) TBLs, as well as in APGs developing on wing sections (Hosseini *et al.*, 2016). The reader is referred to the respective papers for the specific parameters and simulation details. Additionally, an extensive experimental campaign was carried out at the Minimum Turbulence Level (MTL) wind tunnel at KTH Royal Institute of Technology by means of hot-wire anemometry (HWA) and particle image velocimetry (PIV). The desired pressure-gradient conditions and flow histories were established by means of wall inserts, and the wall-shear stress was measured by using oil-film interferometry (OFI). The established pressure gradient and Reynolds number space is displayed in form of  $\beta - Re_\tau$  plots as

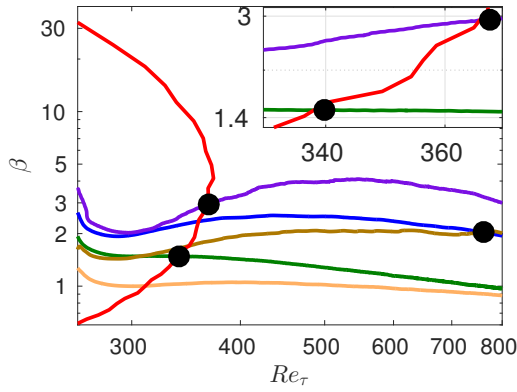


Figure 1. Clauser pressure-gradient parameter  $\beta$  as function of friction Reynolds number  $Re_\tau$  for the following cases: — boundary layer developing on the suction side of a wing (Hosseini *et al.*, 2016), and over a flat plate for non-constant  $\beta$ -cases (—  $m = -0.13$ , —  $m = -0.16$  and —  $m = -0.18$ ) (Bobke *et al.*, 2016) and constant  $\beta$ -cases (—  $\beta = 1$  and —  $\beta = 2$ ) (Bobke *et al.*, 2017).

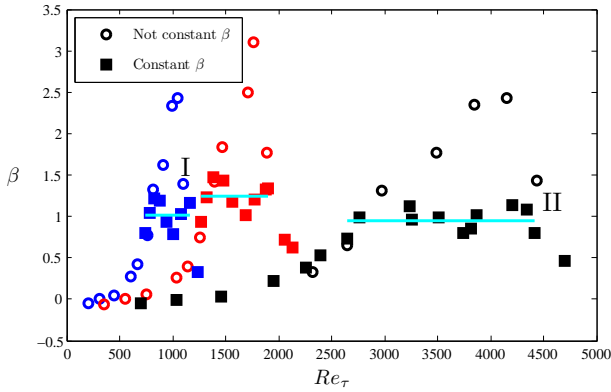


Figure 2. Clauser pressure-gradient parameter distributions in terms of the friction Reynolds numbers for the various constant and non-constant  $\beta$  cases. Experiments were performed with inflow velocities of (blue) 6, (red) 12 and (black) 30 m/s. Comparisons between cases with different  $\beta$  histories are done at (I)  $\beta \simeq 1.2$ ,  $Re_\tau \simeq 1100$  and (II)  $\beta \simeq 1.2$  and  $Re_\tau \simeq 4500$ . Cyan lines indicate the constant- $\beta$  regions.

depicted in Figure 1 and 2 (note that  $Re_\tau$  is the friction Reynolds number, formed with the friction velocity  $u_\tau$  and the 99% boundary-layer thickness  $\delta_{99}$ ), which will later on be utilised to study the impact of particular  $\beta$  distributions on the state of the TBL by considering matching  $\beta$  and  $Re_\tau$  values.

## RESULTS

The streamwise development of the five near-equilibrium APG TBLs on flat plates obtained in the simulations (Figure 1), defined by different power-law exponents and virtual origins, is clearly distinguishable from the trend of the APG TBL on the suction side of a wing when considering the  $\beta - Re_\tau$  plot. While  $\beta$  decreases over the streamwise direction in the cases denoted with  $m$  ( $m13$ ,  $m16$ ,  $m18$ ),  $\beta$  remains constant for the two cases denoted with  $b$  ( $b1$ ,  $b2$ ). Let us recall that although  $\beta$  is not constant with  $x$  in the  $m$  cases, these TBLs are in near-equilibrium due to the fact that the  $U_\infty$  distribution is prescribed by a power law as defined by Townsend (1956)

and Mellor & Gibson (1966). Regarding the cases with constant  $\beta$ , not only are they in near-equilibrium, but they also allow a better characterisation of Reynolds-number effects in a certain pressure-gradient configuration. Note that the ZPG TBL flow essentially corresponds to a constant  $\beta = 0$  configuration. To further extend the Reynolds-number range, six of the experimentally realised  $\beta$  distributions are shown in Figure 2. The effect of the different histories can be assessed when the cases under consideration have the same Reynolds number and APG magnitude, but have been subjected to different accumulated pressure-gradient effects due to the particular  $\beta$  distributions. Such matching conditions have been highlighted in both Figure 1 and 2 and will be discussed in terms of mean and turbulence quantities in the following.

In Figure 3 we show the inner-scaled mean flow for the various comparisons discussed above, as well as selected components of the Reynolds-stress tensor. The first two important observations from this figure are: although the two comparisons are at the same  $\beta$  and  $Re_\tau$ , the turbulence statistics in the outer layer are essentially different among the cases, while they agree in the viscous sublayer. This highlights the significant impact of history effects on the state of the outer layer of a turbulent boundary layer. Focusing on Figure 3(a,c), we can observe the general effect of a moderate APG on the boundary layers, compared with the equivalent ZPG case: the APG TBLs exhibit a steeper logarithmic region, as previously observed by Nagib & Chauhan (2008) who reported lower values of the von Kármán coefficient  $\kappa$  in APGs. Moreover, the APG TBLs also exhibit a more prominent wake than the ZPG, associated with stronger energetic structures in the outer region, as also observed by Monty *et al.* (2011) and Vinuesa *et al.* (2014). Monty *et al.* (2011) and Harun *et al.* (2013) showed that the APG energises the largest turbulent structures in the outer flow, leading to the more prominent wake, as well as to the outer peak in the streamwise velocity fluctuation profile. The most characteristic features of APG TBLs in terms of the Reynolds-stress tensor components become apparent when compared to the ZPG case as shown in Figure 3(b,d) (Monty *et al.*, 2011): the streamwise velocity fluctuation profile develops an outer peak, a consequence of the energising of the large-scale motions, which also produces an increase of the near-wall peak due to the connection between the near-wall region and the outer flow. Note that the location of this inner peak,  $y^+ \simeq 15$ , is essentially unaffected by the APG, and the amplitude of the inner peak appears to be approximately the same in the two cases. The wall-normal and spanwise velocity variance profiles, as well as the Reynolds shear-stress profile, exhibit a more prominent outer region compared to the ZPG due to the effect of the APG on the outer flow.

The previous comparison showed the great impact of the flow history in the state of a TBL, and in particular it highlighted the importance of constant- $\beta$  cases as *canonical* representations of an APG TBL subjected to a certain pressure-gradient magnitude. In Figure 4 the inner-scaled mean velocity profile and selected components of the Reynolds-stress tensor for the cases with constant values of  $\beta = 0, 1$  and  $2$ , *i.e.* the ZPG and two APG cases, are depicted for a matched value of  $Re_\tau \simeq 700$ . The interest of these configurations lies in the fact that they do not depend on flow history, and therefore can be considered as reference results for the corresponding  $\beta$  cases. Thus, the reported differences among cases are uniquely due to the pressure gradient, and not to flow history. The mean flow profile reveals the more prominent wake (connected to a lower skin-friction coefficient) at larger APGs, and also clearly shows the fact that the buffer layer lies below the one of the ZPG TBL, an effect that becomes more pronounced at progressively larger values of  $\beta$ . As opposed to what is observed in stronger APG conditions (Skåre & Krogstad, 1994), the cases under consideration in Figure 4 do not exhibit any differences in the viscous sub-

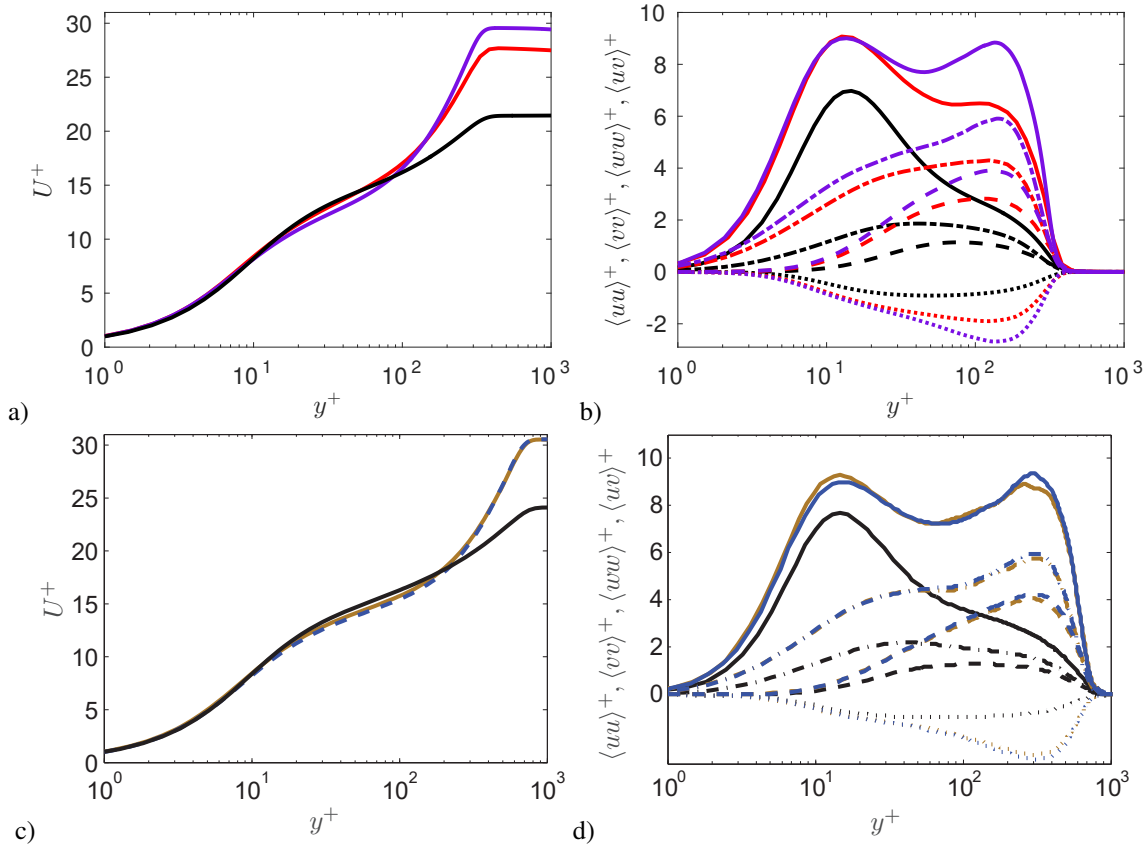


Figure 3. (a), (c) Inner-scaled mean velocity profiles and (b), (d) selected components of the inner-scaled Reynolds-stress tensor. (a), (b) correspond to  $\beta = 2.9$  and  $Re_\tau = 367$ ; and (c), (d) to  $\beta = 2.0$  and  $Re_\tau = 762$ . For colours see caption of Figure 1. Note that the black line corresponds to a ZPG TBL at matched  $Re_\tau$  (Schlatter & Örlü, 2010).

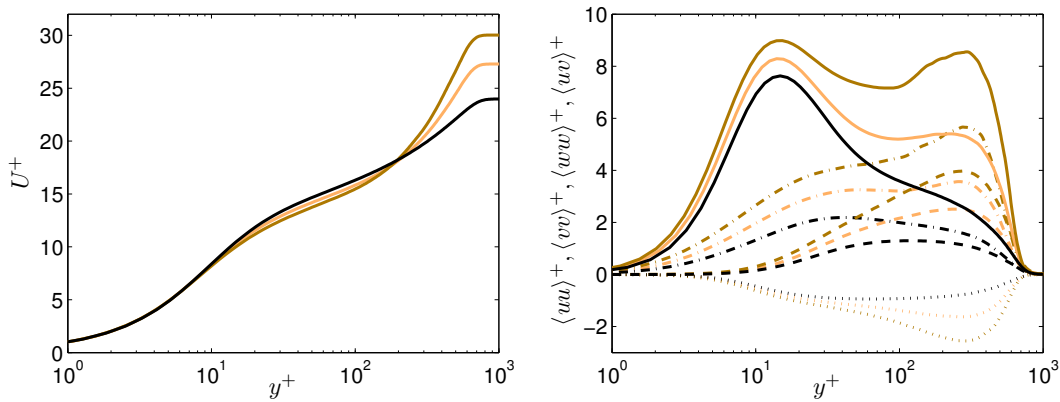


Figure 4. (a) Inner-scaled mean velocity profiles and (b) selected components of the inner-scaled Reynolds-stress tensor. Cases with constant values of  $\beta = 0, 1$  and  $2$ , at matched friction Reynolds number  $Re_\tau \simeq 700$ . For colours see caption of Figure 1.

layer with respect to the ZPG. As discussed above, the APG also has an important effect in the Reynolds-stress tensor components, manifested in more energetic velocity fluctuation profiles, as well as Reynolds shear-stress profiles. This effect also becomes more pronounced for increasing values of  $\beta$ , and in the  $\beta = 2$  case the magnitude of the outer peak in the streamwise velocity fluctuation profile is almost as large as that of the inner peak. An outer peak, which was not present in the ZPG case (but is expected to emerge at higher  $Re$  as discussed in Alfredsson *et al.*, 2011), also emerges

in the other components of the Reynolds-stress tensor, the magnitude of which is proportional to the value of  $\beta$ . Another interesting observation from the Reynolds-stress profiles is the fact that, in the near-wall region, the streamwise and spanwise fluctuation profiles exhibit larger values for progressively stronger APG conditions.

To extend the Reynolds number range further, Figure 5 shows profiles of the inner-scaled streamwise mean and variance from two cases with different history effects, but same  $\beta \simeq 1.2$  and  $Re_\tau \simeq 1100$  and  $4500$ . Note that a ZPG TBL (i.e.  $\beta = 0$ ) profile

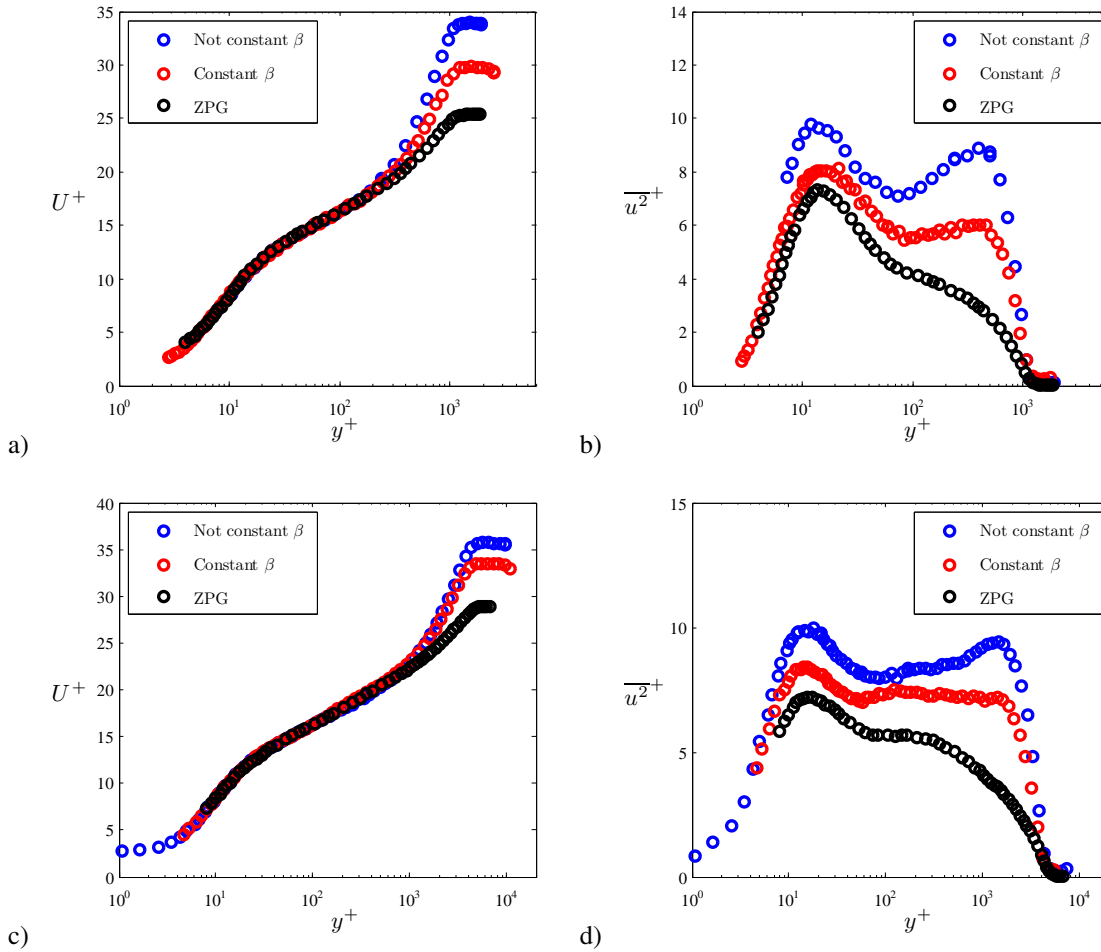


Figure 5. (a), (c) Inner-scaled profiles of the streamwise mean (b), (d) and variance, at case I and II from Figure 2, i.e.  $\beta \simeq 1.2$ ,  $Re_\tau \simeq 1100$  and 4500. ZPG TBL profile (Örlü & Schlatter, 2013) at matched  $Re_\tau$  shown for comparison purposes.

at matched  $Re_\tau$  from Örlü & Schlatter (2013) is shown for comparison. As in the case from the lower Reynolds-number simulations, the results from the two APG cases from the wind-tunnel experiments also do not agree, although the local value of  $\beta$  is the same. The non-constant  $\beta$  case, which has been subjected to stronger APG conditions for a longer streamwise distance, exhibits a more prominent wake in the mean profile, as well as a stronger outer peak in the variance profile than the constant- $\beta$  APG. It can therefore be stated that in order to assess the state of an APG TBL, it is necessary to consider not only the local pressure-gradient conditions, but also the streamwise evolution (or flow history) that led to that particular flow condition.

## SUMMARY AND OUTLOOK

The present study is focused on the history effects in turbulent near-equilibrium boundary layers with adverse pressure gradients. After defining the *near-equilibrium* state according to Townsend (1956), large-eddy simulations were performed over a flat plate to assess the effect of different evolutions of the pressure-gradient parameter  $\beta$ . Hereby constant and non-constant pressure-gradient-parameter distributions were achieved and enabled the separation of Reynolds-number effects and pressure-gradient effects.

Ongoing accompanying studies have shown that APG TBLs with constant values of  $\beta$ , can be described over a certain  $Re$ -range analogous to ZPG TBLs by means of a simple transformation (Vinueza *et al.*, 2017). Furthermore, the aforementioned comparison of com-

ponents of the Reynolds-stress tensor, could also be extended to higher Reynolds numbers by means of the available PIV measurements (Sanmiguel Vila *et al.*, 2017a).

## ACKNOWLEDGEMENTS

Financial support provided by the Knut and Alice Wallenberg Foundation and the Swedish Research Council (VR) is gratefully acknowledged. The simulations were performed on resources provided by the Swedish National Infrastructure for Computing (SNIC) at the PDC Center for High Performance Computing at KTH Stockholm. RÖ acknowledges the financial support of the Lundeqvist foundation.

## DISCLAIMER

Large parts of the present contribution represent a summary and outlook of the authors published and submitted contributions, respectively: Bobke *et al.* (2017), Sanmiguel Vila *et al.* (2017a), and Vinueza *et al.* (2017).

## REFERENCES

- Alfredsson, P. H., Segalini, A. & Örlü, R. 2011 A new scaling for the streamwise turbulence intensity in wall-bounded turbulent flows and what it tells us about the “outer” peak. *Phys. Fluids* **23**, 041702.
- Bobke, A., Vinuesa, R., Örlü, R. & Schlatter, P. 2016 Large-eddy simulations of adverse pressure gradient turbulent boundary layers. *J. Phys.: Conf. Ser.* **708**, 012012.
- Bobke, A., Vinuesa, R., Örlü, R. & Schlatter, P. 2017 History effects and near-equilibrium in adverse-pressure-gradient turbulent boundary layers. *J. Fluid Mech. (In Print)*.
- Harun, Z., Monty, J. P., Mathis, R. & Marusic, I. 2013 Pressure gradient effects on the large-scale structure of turbulent boundary layers. *J. Fluid Mech.* **715**, 477–498.
- Hosseini, S. M., Vinuesa, R., Schlatter, P., Hanifi, A. & Henningson, D. S. 2016 Direct numerical simulation of the flow around a wing section at moderate Reynolds number. *Int. J. Heat Fluid Flow* **61**, 117–128.
- Lee, J.-H. & Sung, H. J. 2008 Effects of an adverse pressure gradient on a turbulent boundary layer. *Int. J. Heat Fluid Flow* **29**, 568–578.
- Maciel, Y., Rossignol, K.-S. & Lemay, J. 2006 Self-Similarity in the outer region of adverse-pressure-gradient turbulent boundary layers. *AIAA J.* **44**, 2450–2464.
- Marusic, I., Mckee, B. J., Monkewitz, P. A., Nagib, H. M., Smits, A. J. & Sreenivasan, K. R. 2010 Wall-bounded turbulent flows at high Reynolds numbers: Recent advances and key issues. *Phys. Fluids* **22**, 065103.
- Mellor, G. L. & Gibson, D. M. 1966 Equilibrium turbulent boundary layers. *J. Fluid Mech.* **24**, 225–253.
- Monty, J. P., Harun, Z. & Marusic, I. 2011 A parametric study of adverse pressure gradient turbulent boundary layers. *Int. J. Heat Fluid Flow* **32**, 575–585.
- Nagib, H. M. & Chauhan, K. A. 2008 Variations of von Kármán coefficient in canonical flows. *Phys. Fluids* **20**, 101518.
- Örlü, R. & Schlatter, P. 2013 Comparison of experiments and simulations for zero pressure gradient turbulent boundary layers at moderate Reynolds numbers. *Exp. Fluids* **54**, 1547.
- Patel, V. C. & Sotiropoulos, F. 1997 Longitudinal curvature effects in turbulent boundary layers. *Prog. Aerosp. Sci.* **33**, 1–70.
- Sanmiguel Vila, C., Örlü, R., Vinuesa, R., Schlatter, P., Ianiro, A. & Discetti, S. 2017a Adverse-pressure-gradient effects on turbulent boundary layers: a PIV study. *Flow Turbul. Combust. (submitted)*.
- Sanmiguel Vila, C., Vinuesa, R., Discetti, S., Ianiro, A., Schlatter, P. & Örlü, R. 2017b On the identification of well-behaved turbulent boundary layers. *J. Fluid Mech. (In Print)*.
- Schlatter, P. & Örlü, R. 2010 Assessment of direct numerical simulation data of turbulent boundary layers. *J. Fluid Mech.* **659**, 116–126.
- Schlatter, P. & Örlü, R. 2012 Turbulent boundary layers at moderate Reynolds numbers. Inflow length and tripping effects. *J. Fluid Mech.* **710**, 5–34.
- Skåre, P. E. & Krogstad, P.-Å. 1994 A turbulent equilibrium boundary layer near separation. *J. Fluid Mech.* **272**, 319–348.
- Townsend, A. A. 1956 *The Structure of Turbulent Shear Flow*. Cambridge Univ. Press, Cambridge, UK.
- Vinuesa, R., Örlü, R., Sanmiguel Vila, C., Ianiro, A., Discetti, S. & Schlatter, P. 2017 Revisiting history effects in adverse-pressure-gradient turbulent boundary layers. *Flow Turbul. Combust. (submitted)*.
- Vinuesa, R., Rozier, P. H., Schlatter, P. & Nagib, H. M. 2014 Experiments and computations of localized pressure gradients with different history effects. *AIAA J.* **55**, 368–384.